Membrane Perturbation Induced by Interfacially Adsorbed Peptides

Assaf Zemel,* Avinoam Ben-Shaul,* and Sylvio May†
*Department of Physical Chemistry and the Fritz Haber Research Center, The Hebrew University of Jerusalem, Jerusalem 91904, Israel; and †Institut für Molekularbiologie, Friedrich-Schiller-Universität Jena, 07745 Jena, Germany

ABSTRACT The structural and energetic characteristics of the interaction between interfacially adsorbed (partially inserted) α-helical, amphipathic peptides and the lipid bilayer substrate are studied using a molecular level theory of lipid chain packing in membranes. The peptides are modeled as ''amphipathic cylinders'' characterized by a well-defined polar angle. Assuming two-dimensional nematic order of the adsorbed peptides, the membrane perturbation free energy is evaluated using a cell-like model; the peptide axes are parallel to the membrane plane. The elastic and interfacial contributions to the perturbation free energy of the ''peptide-dressed'' membrane are evaluated as a function of: the peptide penetration depth into the bilayer's hydrophobic core, the membrane thickness, the polar angle, and the lipid/peptide ratio. The structural properties calculated include the shape and extent of the distorted (stretched and bent) lipid chains surrounding the adsorbed peptide, and their orientational (C-H) bond order parameter profiles. The changes in bond order parameters attendant upon peptide adsorption are in good agreement with magnetic resonance measurements. Also consistent with experiment, our model predicts that peptide adsorption results in membrane thinning. Our calculations reveal pronounced, membrane-mediated, attractive interactions between the adsorbed peptides, suggesting a possible mechanism for lateral aggregation of membrane-bound peptides. As a special case of interest, we have also investigated completely hydrophobic peptides, for which we find a strong energetic preference for the transmembrane (inserted) orientation over the horizontal (adsorbed) orientation.

INTRODUCTION

The broad-spectrum antimicrobial activity of many naturally occurring α-helical amphipathic peptides such as melittin, magainins, cecropins, ovispirin, dermaseptins, and others most likely follows from their strong tendency to adsorb onto lipid membranes and from their capacity to perforate them (Hancock et al., 1995; Nicolas and Mor, 1995; Epand and Vogel, 1999; Yamaguchi et al., 2001). Their activity is not mediated by specific receptors, but rather correlated with a number of characteristic structural motifs. Upon binding to the lipid membrane they fold into an amphipathic α-helix comprising complementary hydrophobic and hydrophilic faces. The hydrophilic face typically includes between two and six cationic charges. Most α-helical antimicrobial peptides are short, with their length comparable to the thickness of a lipid bilayer, namely 20–40 Å (Bechinger, 1997). Due to their nonspecific (i.e., not receptor-mediated) interaction with membranes, amphipathic peptides were suggested as alternatives to conventional antibiotics. This has initiated numerous experimental studies designed to uncover the mechanisms of peptide-induced membrane perforation (Matsuzaki, 1999; Bechinger, 2001; Dathe and Wieprecht, 1999). For many amphipathic peptides, like those mentioned above, solid state NMR, oriented circular dichroism, and Fourier transform infrared spectroscopy (Bechinger, 1999), as well as x-ray measurements (Hristova et al., 2001; White and Wimley, 1998) all support the conclusion that below a threshold peptide/lipid ratio of the order of 1:100 (depending on the lipid and the peptide type), the peptides orient horizontally parallel to the lipid membrane interface, with the polar part inserted between the lipid headgroups and the hydrophobic face buried inside the hydrocarbon core. At this particular spatial orientation, amphipathic peptides modulate the physical properties of the host membrane. This concerns, for example, a decrease of membrane thickness (Ludtke et al., 1995), modifications of the molecular order parameter along the lipid chains (Koenig et al., 1999), the thermotropic phase behavior of the membrane (Jing et al., 2003), or the peptide's propensity to alter the preferred bilayer curvature (Epand, 1997).

Peptide adsorption onto the membrane surface, which is the subject matter of this study, constitutes an essential first step in the membrane perforation mechanism. The interfacially adsorbed amphipathic peptides that self-assemble within the membrane plane eventually aggregate into a ''carpet'' that leads to membrane solubilization in a detergent-like mechanism or undergoes a cooperative transition from the ''horizontal'' (membrane-parallel) orientation to a ''perpendicular'' (membrane-inserted) state, whereby groups of several peptides join to form transmembrane pores (Oren and Shai, 1998; He et al., 1996; Zuckermann and Heimburg, 2001; Zemel et al., 2003).

Notwithstanding the progress in the biophysical characterization of the peptide-dressed membrane, molecular-level understanding of the structural and energetic characteristics of the interaction between amphipathic peptides and lipid membranes is still lacking. To a large extent, this is due to the complexity of the underlying interactions, namely, the electrostatic interactions between the peptide's cationic

Submitted August 21, 2003, and accepted for publication December 18, 2003.

Address reprint requests to Sylvio May, Institut für Molekularbiologie, Winzerlaer Strasse 10, 07745 Jena, Germany. Tel.: 49-3641-657582; E-mail: Silvio.May@uni-jena.de.

0006-3495/04/06/3607/13 $2.00

doi: 10.1529/biophysj.103.033605

residues and the dipolar (or anionic) lipid headgroups, the desolvation of hydrophobic side chains upon penetration into the hydrocarbon core of the host membrane, and conformational changes of the peptide's backbone, as well as changes in the packing properties of the lipid chains in the vicinity of the peptide (White and Wimley, 1998). Modeling of peptide-containing membranes can be helpful in understanding their structural properties and energetics. For example, molecular dynamics simulations provide atomic-level information, typically within timescales of a few up to 100 ns (Shepherd et al., 2003; Lin and Baumgärtner, 2000; La Rocca et al., 1999; Saiz et al., 2002). Often, however, the timescales of interest, e.g., of peptide self-assembly in the membrane plane, are much longer. An alternative (and computationally much less expensive) approach to study membrane-mediated interactions between peptides is provided by continuum, membrane elasticity theories. This approach is commonly applied to transmembrane peptides or proteins (Huang, 1986; Aranda-Espinoza et al., 1996; May and Ben-Shaul, 1999) and has proved to yield useful information for the interpretation of experimental data (Nielsen et al., 1998; Harroun et al., 1999). Its application to interfacially adsorbed peptides requires additional approximations, associated with the lower symmetry of the problem, reflecting the partial penetration of the peptides (as compared to transmembrane) into one monolayer of the membrane (Huang, 1995). Intermediate between the continuum and atomic-level approaches are molecular-level, mean-field theories of conformational chain-packing statistics in lipid membranes, (and other, e.g., micellar, aggregates of amphiphilic molecules). In the past, a theory of this kind has been employed to describe in detail the conformational properties of lipid tails in various aggregation geometries, showing very good agreement with experimental results pertaining to a variety of single molecule properties, e.g., orientational bond order parameters of the lipid tails, as well as thermodynamic membrane characteristics such as the curvature elasticity of lipid bilayers (Ben-Shaul, 1995). This approach has been extended to lipid-protein systems, and used to calculate interaction energies between a lipid bilayer and a membrane-spanning protein (Fattal and Ben-Shaul, 1993), as well as the membrane-mediated interaction between transmembrane proteins (May and Ben-Shaul, 2000).

In this work, we extend and apply this chain-packing theory to a lipid membrane that contains interfacially adsorbed amphipathic peptides. That is, we calculate the contribution of the lipid tails to the membrane-peptide interaction free energy, as a function of the penetration depth of the peptide into the membrane. The α-helical peptides are modeled as cylinder-like rigid molecules that are oriented parallel to the membrane surface. Their optimal penetration depth is determined by the balance between the interfacial (hydrophobic) free energy, which depends on the polar angle (defining the peptide's sector spanned by the hydrophilic residues), and the elastic perturbation free energy of the lipid chains constituting the hydrophobic core of the host membrane. Our approach treats the lipid chain packing within the hydrocarbon core of the membrane in molecular detail; yet, to keep the model computationally feasible, we have employed two significant approximations: first, we impose the membrane to be flat, and second, we assume that the thickness of its hydrophobic core is uniform throughout, i.e., we allow for global but not local modulations in membrane thickness. These additional constraints may result in somewhat higher estimates of the peptide-dressed membrane free energy. However, they should not significantly affect the major conclusions of this study pertaining to three central issues: i), the changes in molecular packing characteristics of the lipid chains surrounding the adsorbed peptides, e.g., their orientational bond order parameters; ii), the peptide-induced modifications of membrane thickness; and iii), the nature of the interaction potential between the adsorbed peptides. Moreover, to compare our calculations with experimental results, we shall focus on the regime of high peptide concentrations where the average interhelical distances between peptides are not much larger than the typical decay length of membrane thickness variations. Membrane elasticity theory predicts that this decay length is in the nanometer range (Harroun et al., 1999), suggesting that local modulations in membrane thickness at high peptide concentrations are minor.

THEORY

We consider a flat lipid bilayer, oriented normal to the z axis of a Cartesian coordinate system, with α-helical amphipathic peptides adsorbed onto one, say the ''external'', monolayer, as is schematically depicted in Fig. 1.

The peptides are modeled as cylinders, whose envelope involves a well-defined polar face subtending the ''hydrophilic'' angle α, and a complementary hydrophobic face of angle $2\pi - \alpha$. Neglecting atomic details, we treat the peptides as rigid cylinders of length D and radius r_P, with their long axis parallel to the bilayer (x, y) plane, and with their hydrophobic sector inserted into the hydrocarbon core of the external monolayer. To account for changes in peptide surface concentration, we adopt a cell model approximation, whereby each adsorbed peptide is associated with a cell containing N lipid chains, reflecting the peptide/lipid ratio $1/N$ for single-

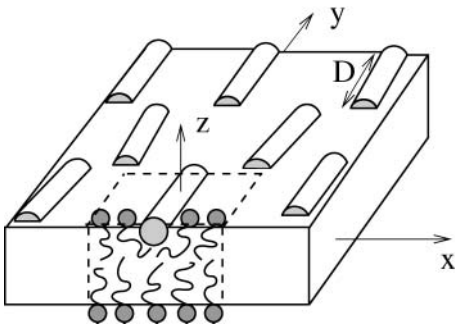

FIGURE 1 Schematic illustration of a lipid bilayer with adsorbed, partially inserted α-helical peptides on its upper (''external'') monolayer. The high peptide concentration results in nematic orientational order of the peptides' long axes. The dashed lines denote the boundaries of a unit cell; some lipids are depicted schematically.

tailed lipids. (The corresponding number for the biologically more relevant double-tailed lipids is $2/N$. Yet, below we shall treat all lipid chains on the same theoretical level so that the distinction between single-tailed and double-tailed lipids becomes irrelevant. For simplicity, we thus shall focus on single-tailed lipids.) Denoting the number of lipid chains in the external monolayer by N_E; the corresponding number in the apposed—peptide free—(''internal'') monolayer, $N_I = N - N_E$, is generally different from N_E. In all the calculations presented below, we shall determine these numbers assuming that the system has reached complete equilibrium (including lipid flip-flop between monolayers).

At high peptide concentration, the interhelical distance L is of order of (possibly even smaller than) the peptide length D. Such a two-dimensional (2D) fluid of membrane-bound peptides should exhibit a long range 2D nematic order (roughly) when L falls below D. Based on this notion, we simplify the definition of our cell model by assuming that all adsorbed peptides are perfectly aligned along one, say the y (the ''director'') axis. For this aligned ensemble of partially inserted peptides, the packing properties of the lipids will mostly depend on the distances between neighboring peptides along the x direction, with minor modulation along the y direction due to modified chain packing around the peptide ends. Neglecting these end effects renders the packing of the lipid molecules uniform in y direction, an approximation that we shall adopt in this work. Accordingly, we treat the membrane properties as translationally invariant along the y direction. The unit cell is a box of dimensions $L \times D \times h$, as depicted in Fig. 2, h denoting the (uniform) thickness of the hydrophobic core.

Geometrical considerations

The volume

$$V = LhD = V_L + V_P \tag{1}$$

of the unit cell involves two contributions. The first, $V_L = Nv$, is the volume occupied by the N lipid tails, each of molecular volume v. In this work we consider fully saturated hydrocarbon chains of the form $-(CH_2)_{13} - CH_3$, (or, in short, C-14 chains). Each methylene group, occupying a volume

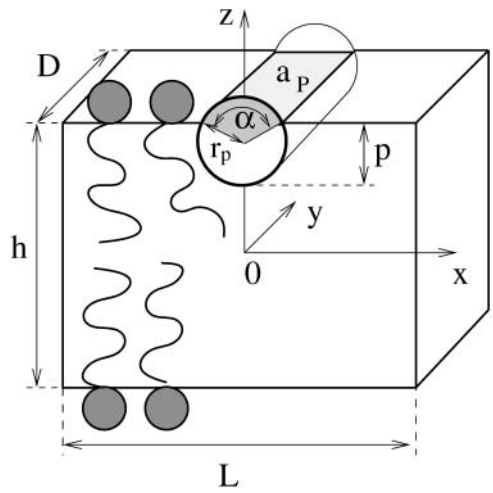

FIGURE 2 Schematic illustration of a lipid bilayer section (the ''unit cell'') containing one, partially inserted, amphipathic peptide. The depth of insertion p defines the insertion angle α corresponding to the peptide sector facing the aqueous environment. In general, this angle is equal to the peptide's polar angle. The (average) interaxial distance between neighboring peptides is L. Note that the thickness of the membrane's hydrocarbon core, h, is assumed to be constant throughout the membrane. Some lipids are depicted schematically.

$\nu \approx 27$ Å^3, is counted as one ''chain segment'' whereas the terminal methyl group is approximately twice as large and will be counted as two chain segments. The chain volume is thus $v \approx 15 \times \nu = 405$ Å^3.

The second contribution to V is that of the membrane-inserted part of the peptide, given by

$$V_P = \frac{r_P^2}{2} D(2\pi - \alpha + \sin\alpha), \tag{2}$$

where α is the ''insertion angle'' defined by the peptide's sector facing the aqueous region. Exposing the peptide's hydrophobic face to the aqueous phase involves a large energetic penalty of magnitude $\gamma_P A_{exp}$, where A_{exp} is the exposed contact area and γ_P the effective (unfavorable) surface tension between the peptide's nonpolar face and the aqueous solution. Although γ_P may vary from one peptide to another (as discussed in more detail below; see Eq. 26), for all reasonable values of γ_P ($\gamma_P \geq 0.02\ k_BT/$Å^2), exposing a significant part of the hydrophobic face to water inflicts an intolerable energetic penalty. Hence, one can safely assume that, at equilibrium, the insertion angle coincides with the peptide's hydrophilic angle, which also implies that this hydrophilic angle dictates the penetration depth, p, of the peptide into the hydrophobic core. Explicitly, $p = r_P[1 + \cos(\alpha/2)]$ (see Fig. 2). Thus, for fixed lipid/peptide ratio (N), and given peptide geometry (r_P and α), Eq. 1 provides a direct relationship between L and h.

Another important geometric determinant is the contact area, A_L, between the lipid tails and the polar environment. It can be expressed as $A_L = 2LD - a_P$, where

$$a_P = 2r_P D \sin(\alpha/2) \tag{3}$$

is the cross-sectional area of the peptide, measured at the interfacial plane, $z = h/2$. The quantity A_L defines the average cross-sectional area per lipid tail, $a_L = A_L/N$, measured at the membrane interfaces ($z = \pm h/2$). Equivalently, it defines the average headgroup density of the lipids, $\overline{\sigma} = 1/a_L = N/A_L$ (recall that we consider single-tailed lipids; for double-tailed lipids, $\overline{\sigma}$ should be multiplied by 1/2).

The free energy

For any given geometry of the unit cell, as specified by N, p, and h (or, equivalently, D, L, and h), we write $F = F(N, p, h)$, the free energy per unit cell (equivalently, per peptide), as a sum of two contributions

$$F = F_i + F_c. \tag{4}$$

The first term, F_i, arises from the (unfavorable) interfacial energy associated with the exposure of hydrophobic lipid chain segments to the aqueous environment. As usual, this energy is modeled here using the familiar simple form,

$$F_i = N\gamma a_L, \tag{5}$$

where $A_L = Na_L$ is the overall hydrocarbon-water contact area and γ is the surface tension, which should be on the order of the oil-water interfacial tension, i.e., $\gamma \approx 0.1\ k_BT/$Å^2, where k_B is Boltzmann's constant and T the absolute temperature. Note that the area per lipid chain, a_L, depends on both h and p.

The second contribution, F_c, arises from the peptide-induced perturbation to the packing properties of the lipid chains within the membrane. In the presence of a peptide, the conformational free energy of a given lipid chain depends on its position along the x axis: $f_c^E = f_c^E(x)$ and $f_c^I = f_c^I(x)$ for lipids

originating from the external and internal monolayer, respectively. Denoting the corresponding 2D densities of lipid headgroups along the x axis by $\sigma_E(x)$ and $\sigma_I(x)$, we express F_c as an integral over the local contributions from all lipids within the unit cell

$$F_c = D\int_{-L/2}^{L/2} dx[\sigma_E(x)f_c^E(x) + \sigma_I(x)f_c^I(x)]. \quad (6)$$

In the peptide-free membrane, all lipids share the same conformational properties, and hence $f_c^E(x) = f_c^I(x) = f_c$ is constant and $F_c = F_c^0(h) = Nf_c(h)$ only depends on the membrane thickness h. Note that, generally, the headgroup densities of the lipids, $\sigma_E(x)$ and $\sigma_I(x)$, must comply with the conservation of the number $N = A_L\overline{\sigma}$ of lipids within the unit cell, implying

$$N = D\int_{-L/2}^{L/2} dx[\sigma_E(x) + \sigma_I(x)]. \quad (7)$$

Clearly, since lipid headgroups cannot enter the surface region occupied by the peptide, $\sigma_E(x) \equiv 0$ in this region, corresponding to $|x| \le a_P/2D = r_P \sin(\alpha/2)$.

The conformational free energy per lipid chain originating at position x of the external monolayer, $f_c^E(x)$ can be expressed in the form (May and Ben-Shaul, 2000)

$$\begin{aligned} f_c^E(x) &= k_BT\ln\frac{\sigma_E(x)}{\overline{\sigma}} + \sum_\alpha P_E(\alpha \mid x)[\epsilon(\alpha) \\ &\quad + k_BT\ln P_E(\alpha \mid x)] \\ &= k_BT\ln\frac{\sigma_E(x)}{\overline{\sigma}} + \langle\epsilon(\alpha)\rangle_E - T\langle s\rangle_E \end{aligned} \quad (8)$$

The first term here accounts for the ''demixing'' (translational) entropy of the headgroups with respect to the uniform distribution, $\overline{\sigma}$. The second contribution is the conformational free energy per lipid. It involves the conditional probability, $P_E(\alpha \mid x)$, of a lipid chain anchored at position x of the external monolayer to be found in conformation α. The conditional probability is normalized, $\sum_\alpha P_E(\alpha \mid x) = 1$, for all accessible x. The summation in Eq. 8 runs over all possible chain conformations, specified by the positions of all chain segments that constitute the chain; $\epsilon(\alpha)$ is the corresponding internal (*trans*/*gauche*) energy of the chain. Excluded from the sum are all chain conformations for which one or more chain segments protrude beyond the hydrophobic core into the aqueous environment. Similarly, we discard all conformations ''intersecting'' the peptide's boundaries.

We identify $\langle\epsilon(\alpha)\rangle_E = \sum_\alpha P_E(\alpha \mid x)\epsilon(\alpha)$ as the average internal energy of a chain attached to the external monolayer at position x. Similarly, $\langle s\rangle_E = -k_B\sum_\alpha P_E(\alpha \mid x)\ln P_E(\alpha \mid x)$ is the conformational entropy of this chain. Note that $\langle\epsilon(\alpha)\rangle_E = \langle\epsilon(\alpha)\rangle_E(x)$ and $\langle s\rangle_E = \langle s\rangle_E(x)$ depend on the anchoring position x of the chain origin. Particularly, the presence of a rigid and impenetrable peptide reduces the number of accessible chain conformations for the lipids in the vicinity of the peptide. Consequently, we expect $\langle s\rangle_E$ to be larger for lipids farther away from the peptide. Note finally that an analogous expression as for $f_c^E(x)$ is also valid for $f_c^I(x)$.

The conformational free energy, F_c (unlike $F_i = F_i(h, p)$), depends on the functions $\sigma_E(x)$, $\sigma_I(x)$, $P_E(\alpha|x)$, and $P_I(\alpha|x)$. In thermodynamic equilibrium, F_c is minimal with respect to these quantities, subject to all relevant constraints. As in previous applications of this formalism, we impose only one packing constraint, namely, that of uniform density everywhere within the hydrocarbon core, reflecting the liquid-like nature of the lipid bilayer. The hydrophobic chain region is thus treated as a fluid-like, incompressible medium with uniform density of chain segments throughout. This assumption is not affected by the presence of the peptide. The peptide only excludes a region of the lipid bilayer from being part of the hydrocarbon core and (or) headgroup region.

We emphasize that the condition of uniform chain packing is our only constraint in the minimization of F_c. Thus, the headgroup densities, $\sigma_E(x)$ and $\sigma_I(x)$, can freely adjust, ensuring an optimal lipid distribution, $N_E = D\int_{-L/2}^{L/2} dx\sigma_E(x)$ and $N_I = D\int_{-L/2}^{L/2} dx\sigma_I(x)$, within the two monolayers. In other words, our approach accounts for optimal flip-flop of the lipids between the two bilayer leaflets.

For the mathematical expression of the uniform density constraint, consider a small volume element $d^3\mathbf{r}$ at position $\mathbf{r}$ within the hydrocarbon core. Denote by $\phi_E(\alpha, x; \mathbf{r})$ the density of chain segments at position $\mathbf{r}$, due to a lipid chain in conformation α whose headgroup is anchored at position x of the external monolayer. The density of chain segments at $\mathbf{r}$, contributed by all lipids from both the external and internal monolayer is then

$$\begin{aligned} \langle\phi(\mathbf{r})\rangle = \frac{D}{N}\int_{-L/2}^{L/2} dx\Big\{&\sigma_E(x)\sum_\alpha P_E(\alpha \mid x)\phi_E(\alpha, x; \mathbf{r}) \\ &+ \sigma_I(x)\sum_\alpha P_I(\alpha \mid x)\phi_I(\alpha, x; \mathbf{r})\Big\}, \end{aligned} \quad (9)$$

where $\phi_I(\alpha, x;\mathbf{r})$ is defined in analogy to $\phi_E(\alpha, x; \mathbf{r})$. The constraint of uniform chain segment density within the entire hydrocarbon chain region is thus

$$\langle\phi(\mathbf{r})\rangle = \overline{\phi} = \frac{1}{\nu N} \quad (10)$$

for all positions $\mathbf{r}$ within the hydrocarbon core.

Minimization (in fact, functional minimization) of $F_c = F_c[\sigma_E(x), \sigma_I(x), P_E(\alpha \mid x), P_I(\alpha \mid x)]$ subject to Eq. 10 leads to the (local, at x) probability distribution of chain conformations as was previously derived by May and Ben-Shaul (2000),

$$P_E(\alpha \mid x) = \frac{1}{q_E(x)}\chi_E(\alpha, x), \quad (11)$$

with the generalized Boltzmann factor

$$\chi_E(\alpha, x) = \exp\Big\{-\frac{\epsilon(\alpha)}{k_BT} - \int_{V_L} d^3\mathbf{r}\lambda(\mathbf{r})\phi_E(\alpha, x; \mathbf{r})\Big\}. \quad (12)$$

The normalization, $\sum_\alpha P_E(\alpha \mid x) = 1$, is ensured by

$$q_E(x) = \sum_\alpha \chi_E(\alpha, x) \quad (13)$$

representing the partition function per lipid chain, attached at position x to the external monolayer. Analogous expressions of $P_I(\alpha|x)$, $\chi_I(\alpha, x)$, and $q_I(x)$ hold for the internal monolayer.

The (dimensionless) function $\lambda(\mathbf{r})$, appearing in Eq. 12, represents the Lagrangian multipliers conjugate to the constraint in Eq. 10. Because uniform chain segment density is imposed at each position $\mathbf{r}$ within the hydrocarbon core, the integration $\int_{V_L} d^3\mathbf{r}$ must run over the entire volume $V_L = Nv$ occupied by the N lipid chains of the unit cell.

Minimization of F_c also leads to the equilibrium headgroup distributions

$$\sigma_E(x) = \overline{\sigma}\frac{q_E(x)}{q}, \quad \sigma_I(x) = \overline{\sigma}\frac{q_I(x)}{q} \tag{14}$$

with

$$q = \overline{\sigma}\frac{D}{N}\int_{-L/2}^{L/2} dx[q_E(x) + q_I(x)] \tag{15}$$

representing the partition function of the entire unit cell of the lipid bilayer. Again, the partition function ensures proper normalization: inserting Eqs. 14 into Eq. 15 recovers Eq. 7.

Calculation of the chain conformational properties, specified by $P_E(\alpha|x)$ and $P_I(\alpha|x)$, and of the headgroup densities, $\sigma_E(x)$ and $\sigma_I(x)$, requires the determination of the Lagrangian multipliers, $\lambda(\mathbf{r})$, at each point within the volume, V_L, of the hydrocarbon core. The function $\lambda(\mathbf{r})$ is obtained by solving the self-consistency equations

$$0 = \int_{-L/2}^{L/2} dx\Big\{\sum_\alpha \chi_E(\alpha,x)[\phi_E(\alpha,x;\mathbf{r}) - \overline{\phi}] + \sum_\alpha \chi_I(\alpha,x)[\phi_I(\alpha,x;\mathbf{r}) - \overline{\phi}]\Big\}, \tag{16}$$

which are obtained by inserting $P_E(\alpha|x)$, $P_I(\alpha|x)$, $\sigma_E(x)$, and $\sigma_I(x)$ (see Eq. 11 and Eqs. 14) into the constraint $\langle\phi(\mathbf{r})\rangle = \overline{\phi}$ (see Eq. 10) with the average $\langle\phi(\mathbf{r})\rangle$ defined in Eq. 9.

The self-consistency equations are a coupled set of transcendental equations for the function $\lambda(\mathbf{r})$ at all points $\mathbf{r}$ that are enclosed within V_L. The numerical procedure, employed to solve Eqs. 16, is based on a discretization scheme and has been described in previous work (May and Ben-Shaul, 2000).

Once $\lambda(\mathbf{r})$ is known, we can calculate the conformational free energy, F_c, of the membrane per peptide. Introducing the expressions for $P_E(\alpha \mid x)$, $P_I(\alpha \mid x)$, $\sigma_E(x)$, and $\sigma_I(x)$ into F_c, we arrive (after some algebra) at

$$\frac{F_c}{Nk_BT} = -\ln q - \overline{\phi}\int_{V_L} d^3\mathbf{r}\lambda(\mathbf{r}). \tag{17}$$

A convenient reference state for calculating the free energy is the peptide-free bilayer. In this case, all physical quantities are constant along the x axis (as they are along the y axis), i.e., $q_E(x) = q_I(x) = q$ and $\sigma_E(x) = \sigma_I(x) = \overline{\sigma}$, etc.; and the Lagrangian parameters, $\lambda(\mathbf{r}) \to \lambda(z)$, depend only on the normal direction (the z direction) of the membrane. As already mentioned above, the corresponding free energy then depends only on the membrane thickness, h, and will be denoted by $F_c^0(h)$. Similarly, the overall free energy for the peptide-free membrane (containing N lipids) will be denoted by $F^0(h)$.

RESULTS AND DISCUSSION

In this section, we present and discuss the results of calculations pertaining to a number of central conformational lipid chain properties, as well as the free energies of peptide-dressed lipid bilayers. In all calculations, we use $r_P = 6$ Å for the radius of the cylindrical peptide rod, and $D = 30$ Å for its length. As already mentioned, we shall present all results for C-14 lipid chains, each of which occupies a volume of $v = 405$ Å^3 within the hydrophobic core in its liquid state. We shall use $\gamma = 0.08\ k_BT/$Å^2 for the surface tension corresponding to the hydrocarbon-water interface.

Single-chain properties

The average cross-sectional area per lipid chain (equivalently per lipid headgroup for single-tailed lipids) in an unperturbed (peptide-free) bilayer is typically in the range $a_L = 30 - 35$ Å^2; for concreteness, we choose $a_L = 31.2$ Å^2, implying a thickness $h^* = 2\ v/a_L = 26$ Å of the hydrocarbon core.

Consider now a peptide-containing membrane with lipid/peptide ratio $N = 80$ (or, equivalently, $N = 40$ for double-chained lipids). This choice is motivated by recent experimental investigations in which similar lipid/peptide ratios were used (Koenig et al., 1999; Ludtke et al., 1995; Chen et al., 2003). The extension, L, of the corresponding unit cell along the x axis is $L = (vN + V_P)/(hD)$ (see Eq. 1). For example, the specific choice $h = h^* = 26$ Å and $\alpha = \pi$ results in (see Eq. 2) $V_P = \pi r_P^2 D/2$ and thus $L = 44$ Å. Hence, our choice $N = 80$ is representative for high peptide concentrations because the interhelical distance compares with the peptide length and with the perturbation decay length as illustrated in Fig. 4 below. We note, however, that even higher peptide concentrations with $1/N \approx 1/10$ are commonly used in solid-state NMR investigations (Yamaguchi et al., 2001; Bechinger, 1999). Fig. 3 shows for $N = 80$ a cross section of the bilayer within the x, z plane, where for some arbitrarily chosen chain origins the average

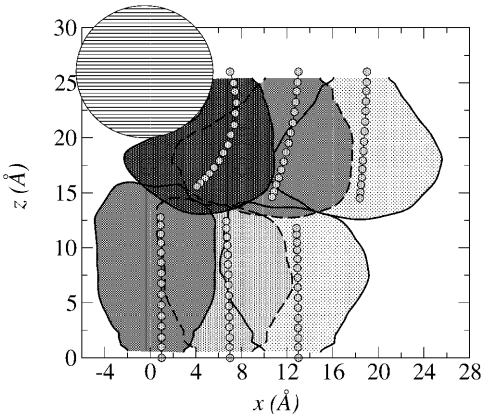

FIGURE 3 The perturbation of a lipid bilayer induced by an amphipathic peptide rod (*hatched circle*) of radius $r_P = 6$ Å and insertion (polar) angle $\alpha = \pi$. Shown is a cross section of (one half of) a unit cell in the x, z plane; the peptide axis is oriented along the y direction. The membrane thickness is $h = 26$ Å, and the lipid/peptide ratio is $N = 80$, implying $L = 44$ Å. For some arbitrarily chosen headgroup locations (*small circles* at $z = 0$ and $z = 26$ Å) along the x axis, the strings of connected circles represent the calculated average positions of the (15, including the one marking the headgroup position) segments, of six representative lipid chains; three from each leaflet. The shaded regions surrounding the chains represent the shape of the volumes accounting for 85% of their possible conformations—qualitatively describing the chain extensions; see text for further explanations.

positions of the chain segments are displayed; 15 per chain, corresponding to C-14 chains, with the first segment denoting the headgroup position. Also shown are—for the same chain origins x—the regions (shaded areas) within which the corresponding lipid chain is found with a probability of 85%. The calculation of this probability is based on the probability density, $P_{\mathrm{E}}^{\mathrm{c}}(\mathrm{r} \mid x)$, of a lipid chain attached at position x to the external monolayer

$$P_{\mathrm{E}}^{\mathrm{c}}(\mathbf{r} \mid x) = \frac{\nu}{v} \sum_{\alpha} P_{\mathrm{E}}(\alpha \mid x) \phi_{\mathrm{E}}(\alpha, x; \mathbf{r}), \tag{18}$$

where we recall that $v/\nu = 15$ is the number of segments per chain, (with the volume taken up by a CH_3 counting as twice the volume per CH_2 group, ν). Similar considerations apply for the internal monolayer. For each position, x, at the hydrocarbon interface, the probability density, $P_{\mathrm{E}}^{\mathrm{c}}(\mathbf{r} \mid x)$, fulfills the normalization condition

$$\int_{V_{\mathrm{L}}} P_{\mathrm{E}}^{\mathrm{c}}(\mathbf{r} \mid x) d^3\mathbf{r} = 1. \tag{19}$$

The shaded areas in Fig. 3 enclose a volume $V_{\mathrm{L}}^{\mathrm{c}}$ whose boundary points fulfill $P_{\mathrm{E}}^{\mathrm{c}}(\mathbf{r} \mid x) = const$, and for which $\int_{V_{\mathrm{L}}^{\mathrm{c}}} P_{\mathrm{E}}^{\mathrm{c}}(\mathbf{r} \mid x) d^3\mathbf{r} = 0.85 \pm 0.02$.

Clearly, and as illustrated in Fig. 3, those chains in immediate vicinity of the peptide must bend strongly to fill up the hydrophobic core region ''under'' the adsorbed peptide. Yet, lipid chains attached to the apposed (the internal) monolayer are also affected by the presence of the peptide. In fact, those chains opposite to the peptide ($|x| \lesssim 10$Å) are significantly stretched (on average) to help fill up the space just under the peptide rod. Bending and stretching of the lipid chains is accompanied by an increase of the headgroup densities, $\sigma_{\mathrm{E}}(x)$ and $\sigma_{\mathrm{I}}(x)$, of the external and internal monolayer, respectively, as is shown in Fig. 4. In other words, the average cross-sectional area per lipid, a_{L}, decreases as the chain origin gets closer to the peptide. This effect is present in both monolayers but is more pronounced in the external (peptide-hosting) one. Note that (the generally repulsive) direct headgroup interactions (which are not taken into account in this work) could lead to a somewhat less pronounced modulation profile than that shown in Fig. 4. Still, the tendency of the lipid headgroups to increase their density near interfacially adsorbed peptides should be a general conclusion, irrespective of their interaction strength.

Furthermore, Fig. 4 shows that the decay length of the lipid perturbation extends 30–40 Å away from the peptide. This implies that any local curvature deformation must relax within this range. A somewhat larger decay length of 62 Å was estimated based on a recent x-ray experiment performed with 1,2-dimyristoyl-*sn*-glycero-3-phosphatidylcholine bilayer interacting with the antimicrobial peptide magainin 2

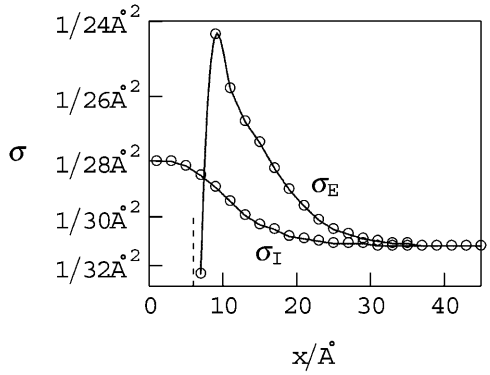

FIGURE 4 Density of headgroups, $\sigma_{\mathrm{E}}(x)$ and $\sigma_{\mathrm{I}}(x)$, in the external and internal monolayers, respectively, calculated for the lipid bilayer corresponding to that in Fig. 3. Note, to obtain the full spatial extension of headgroup density modulations, the results shown here are for a single peptide in a large membrane, i.e., for the limit $N \to \infty$; the results obtained for $N = 80$ are essentially the same.

(Münster et al., 2002). The reason for our somewhat lower estimate might be due to the mean-field character of the approach, which neglects lipid chain correlations.

An experimentally measurable quantity that provides rather direct information pertaining to lipid chain conformational properties is the orientational bond order parameter profile of the lipid tail, usually obtained via NMR measurements of selectively deuterated C-H bonds. The orientational order parameter of, say, the C-H bonds of carbon atom n along the chain is given by

$$S_{\mathrm{n}} = \frac{1}{2}(3\langle \cos^2 \theta_{\mathrm{n}} \rangle - 1), \tag{20}$$

where θ_{n} is the angle between the C_n-H bond and the z axis. In a peptide-free membrane, where all lipid chains are equivalent, the averaging in Eq. 20 involves all possible conformations of any one of the equivalent lipid chains. In the perturbed membrane, the order parameter profiles depend on the chain origin, x. Since the experimentally measured order parameters profiles involve averaging over all lipid chains, we adopt a similar averaging for calculating the S_{n}'s—that is, the averaging involves all conformations of all lipids in both monolayers (as in Eq. 9). Note that a random distribution of bond orientations leads to $S_{\mathrm{n}} = 0$, whereas for a fully stretched (all *trans*) chain oriented along the membrane normal, $-S_{\mathrm{n}} = 1/2$.

Fig. 5 shows $-S_{\mathrm{n}}$ for peptide-containing membranes of various hydrophobic thicknesses, h, and peptide penetration depths, p. Recall that $p = r_{\mathrm{P}}[1 + \cos(\alpha/2)]$ reflects the angular size, α, of the peptide's sector facing the aqueous phase. Larger values of p imply deeper penetration: $p = r_{\mathrm{P}} =$ 6 Å corresponds to $\alpha = \pi$ (see Fig. 3), and for $p > 12$ Å the peptide ($\alpha = 0$) is fully embedded within the hydrocarbon core. Note that for $p = 12$ Å, the peptide resides only within

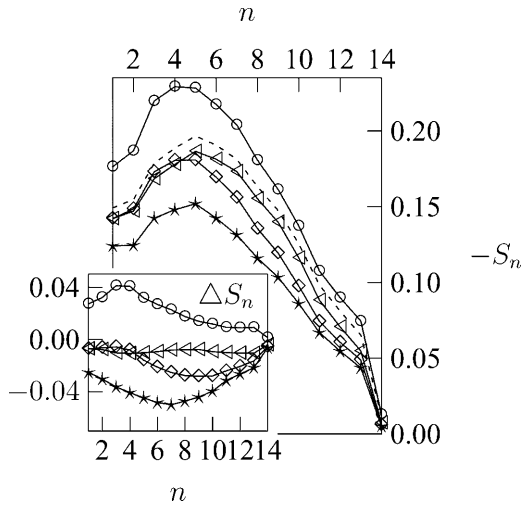

FIGURE 5 Calculated C-H bond order parameter, $-S_n$, for various hydrophobic thicknesses h and peptide penetration depths p. The different curves refer to $h = 26$ Å, $p = 6$ Å (○); $h = 26$ Å, $p = 14$ Å (◁); $h = 24$ Å, $p = 6$ Å (◇); and $h = 26$ Å, $p = 20$ Å (★). The values $S_n = S_n^0$, for an unperturbed (peptide-free) bilayer of hydrophobic thickness $h = h^* = 26$ Å, are indicated by the dashed line. The inset shows the corresponding differences in order parameter, $\triangle S_n = S_n - S_n^0$, relative to the unperturbed, peptide-free bilayer.

one (namely the external) monolayer, just tangent to the upper hydrocarbon-water interface, whereas for $p = h/2 + r_P$, its center is at the bilayer's midplane. Fig. 5 compares $-S_n$ for different peptide penetration depth; $p = 6$ Å (*solid curve* with *open circles*), $p = 14$ Å (*arrowheads*), and $p = 20$ Å (*stars*), with corresponding thickness $h = h^* = 26$ Å of the hydrocarbon core. For comparison, we also show the C-H bond order profile of the peptide-free membrane, $S_n = S_n^0$, membrane (*dashed curve*). The peptide-induced change in the C-H bond order parameter

$$\triangle S_n = S_n - S_n^0 \tag{21}$$

is shown in the inset of Fig. 5: $p = 6$ Å increases the order of the chain ($\triangle S_n > 0$), $p = 14$ Å leaves it unaffected ($\triangle S_n \approx 0$), and $p = 20$ Å disorders the lipid tails ($\triangle S_n < 0$).

The peptide-dressed membrane can lower its free energy by adjusting the thickness, h, of its hydrocarbon core. Analyzing the possibility of membrane thickness variations, more specifically the peptide-induced membrane thinning, is one of the main goals of this work. Fig. 5 shows for $p = 6$ Å (*curves* with *open circles* and *diamonds*) how membrane thinning from $h = 26$ Å to $h = 24$ Å affects S_n and $\triangle S_n$. Clearly, even a change in membrane thickness as small as 1 Å per monolayer thoroughly affects S_n. Particularly, for $h = 24$ Å, those chain segments in the middle of the chain exhibit less orientational order than in an unperturbed membrane, whereas the segments near the headgroups and near the chain ends are marginally affected. Qualitatively the same behavior—including a peptide-induced thinning of the chain region of roughly $h^* - h \lesssim 1$ Å—has been observed experimentally by Koenig et al. (1999), based on deuterium order parameter profiles for membrane-bound amphipathic peptide fragments of the envelope protein of human immunodeficiency virus Type I (HIV-1). Comparable results have also been obtained in a recent molecular dynamics simulation of two antimicrobial peptides in the presence of a lipid bilayer, (Shepherd et al., 2003). Membrane thickness and chain order parameters are seen to decrease as the peptide penetrates into the membrane. The order parameter profiles plotted for the last 10 ns (where the peptide already penetrates the hydrophobic core of the membrane) are in good qualitative and quantitative agreement with our thermodynamic calculations.

The C-H bond order parameters, shown in Fig. 5 represent averages over all lipids within the membrane. That is, all spatial information is averaged out. Yet, our theoretical approach also allows us to compute the order parameters for lipids that reside at specific x positions in either the external or internal monolayer. In this case, the averaging in Eq. 20 is carried out as introduced in Eq. 8 for either the external or internal monolayer.

Fig. 6 shows $-S_n$ for those lipids that are displayed in Fig. 3 (from Fig. 3, we recall $p = 6$ Å and $h = h^* = 26$ Å). There are distinct differences between the chains in the external and internal monolayer. Those attached close to the peptide at the external monolayer exhibit nonmonotonic modulations of S_n compared to S_n^0: Chain segments near the headgroup are more ordered, and chain segments at the methyl end are less ordered compared to an unperturbed lipid tail (*dashed curves* in Figs. 5 and 6). The former is a manifestation of the rigidity of the peptide backbone, and the latter reflects the bending of the lipid tails needed to fill the space below the membrane-penetrating peptide face. On the other hand, lipids ori-

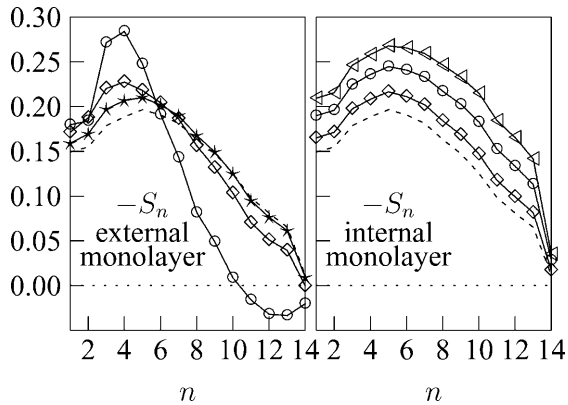

FIGURE 6 C-H bond order parameters, $-S_n$, calculated for lipid chains residing at positions $x = 1$ Å (◁), $x = 7$ Å (○), $x = 13$ Å (◇), and $x = 19$ Å (★). As a comparison, the dashed lines show $-S_n$ for an unperturbed lipid layer. The calculation was performed for $p = 6$ Å and $h = h^* = 26$ Å; the left and right panels refer to the external and internal monolayer, respectively. Note that the selected x positions in each monolayer match those for which the chains are displayed in Fig. 3.

ginating in the internal monolayer show a monotonic increase in $-S_n$ everywhere along the chain. The increase is most pronounced at $x \approx 0$ and follows from the peptide-induced stretching of the chains as evidenced by Fig. 3 and $\sigma_I(x)$ in Fig. 4.

Membrane thinning

Being fluid-like soft materials, lipid membranes are able to adjust their thickness, h, upon the insertion of rigid peptides into the hydrocarbon core. The degree of adjustment is determined by the minimum in free energy $F(N, p, h)$ with respect to h, for any given peptide insertion depth, p, and lipid/peptide ratio, N. Recall that F consists of two contributions (see Eq. 4): the interfacial free energy $F_i = F_i(N, p, h)$ and the chain conformational free energy $F_c = F_c(N, p, h)$. The former, $F_i = N\gamma a_L$, depends on the average cross-sectional area per lipid chain $a_L = a_L(N, p, h)$, which can be calculated as discussed in the Theory section. Because we focus on high peptide concentration, we continue to use $N = 80$ for the lipid/peptide ratio. In the upper panel of Fig. 7, we show a_L as a function of p for different values of h (with 22 Å $\leq h \leq$ 30 Å). If the peptide does not enter into the hydrocarbon core of the membrane (that is, $p \leq 0$) then $a_L = 2\,v/h$. Upon entry, a_L initially decreases and then increases, which reflects the cylinder-like shape of the peptide. For $2\,r_P \leq p \leq h$, the peptide is fully inserted and $a_L = 2(v+\pi r_P^2 D/N)/h$ is constant and higher than for $p = 0$. Generally, larger h gives rise to smaller a_L. Note also the symmetry $a_L(p) = a_L(h + 2r_P - p)$.

The second quantity that enters into F is the conformational free energy of the lipid chains $F_c(p, h)$. (Because $N = 80$ is fixed, we omit the argument N from F_c.) In the lower panel of Fig. 7, we display results of our numerical calculations for the average conformational free energy per lipid chain

$$\frac{\triangle F_c(p,h)}{N} = \frac{F_c(p,h) - F_c^0(h^*)}{N} \qquad (22)$$

measured with respect to an unperturbed (peptide-free) membrane of thickness $h = h^* = 26$ Å, as a function of p for different values of h. The definition of the reference energy, $F_c^0(h^*)$, implies $\triangle F_c(p = 0, h = h^*)/N = 0$. Note that the behavior of $\triangle F_c(p, h)$ is somewhat opposite to that of $a_L(p, h)$. Increasing the membrane thickness, h, induces the lipid chains to be more stretched on average; the corresponding loss of conformational freedom implies higher conformational free energy. In addition to that, upon entry of the peptide into the hydrocarbon core, $\triangle F_c(p)$ initially increases and then decreases. The maximal conformational perturbation of the lipid bilayer is found for $p \approx r_P$, where half of the peptide body is inserted into the host membrane. This case involves a particularly drastic energy penalty for membranes of large thickness, h. No such increase in $\triangle F_c$ is found for fully inserted peptides ($2r_P \leq p \leq h$) or for thin membranes. Already these considerations suggest that membrane thinning could be a mechanism to avoid the high conformational energy penalty associated with interfacially associated amphipathic peptides.

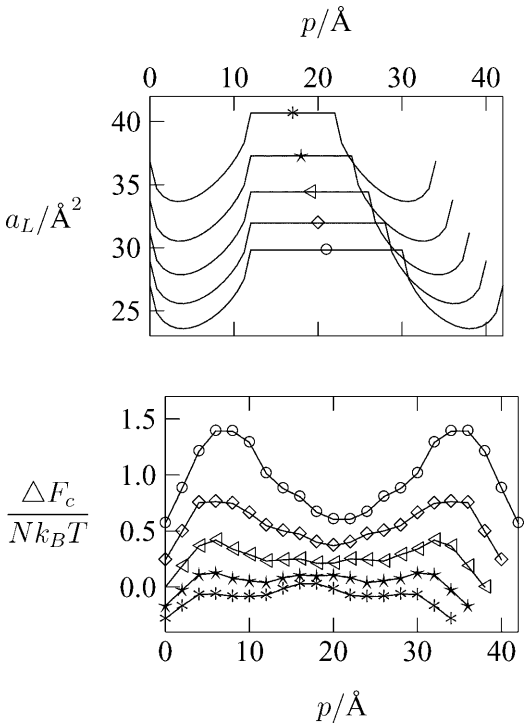

FIGURE 7 Average cross-sectional area per lipid tail a_L (*upper panel*) and average conformational free energy per lipid tail, $\triangle F_c(p, h)/N$, measured with respect to an unperturbed (peptide-free) membrane of thickness $h = h^* = 26$ Å (*lower panel*). In both panels. the different curves refer to $h = 22$ Å (*), $h = 24$ Å (★), $h = 26$ Å (◁), $h = 28$ Å (◇), and $h = 30$ Å (○). All calculations are based on a lipid/peptide ratio of $N = 80$. The curves are plotted as a function of the peptide's penetration depth, p (see Fig. 2), starting at $p = 0$ and ending at $p = h + 2r_P$ for which the peptide is translocated through the whole hydrocarbon core of the bilayer.

The two panels in Fig. 7 contain all relevant information to calculate the free energy per peptide of the membrane, $F(p, h) = N\gamma a_L + F_c$. As for F_c, we shall define an excess free energy through

$$\triangle F(p, h) = F(p, h) - F^0(h^*). \qquad (23)$$

That is, we use as a reference state that of an unperturbed, peptide-free bilayer with corresponding free energy $F^0(h^*) = F(p = 0, h = h^*)$. The effective surface tension, γ, is chosen such that the membrane thickness $h = h^* = 26$ Å represents the equilibrium value of an unperturbed, peptide-free bilayer. In Fig. 8 (the *curve* marked by *open circles*), we demonstrate that this is the case for $\gamma = 0.08\ k_BT/\text{Å}^2$ (which is somewhat smaller than the oil-water interfacial tension of ≈0.12

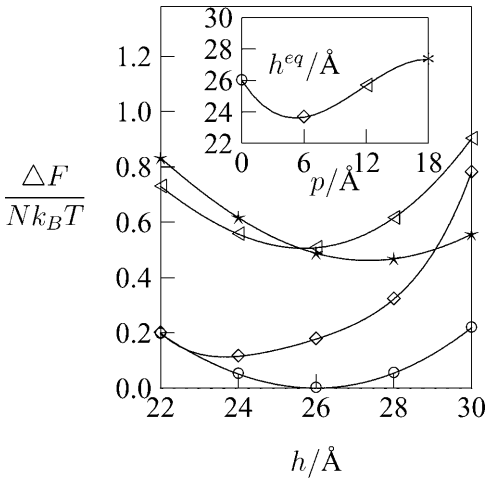

FIGURE 8 The excess free energy per lipid chain, $\triangle F(p, h)/N$ (see Eq. 23) with $\gamma = 0.08 k_B T/$Å^2, as a function of membrane thickness h for a peptide-free membrane (○), for $p = 6$ Å (◇), for $p = 12$ Å (◁), and for $p = 18$ Å (★). At any given peptide penetration depth, p, there is one particular membrane thickness, $h = h^{eq}$, for which $\triangle F(p, h)/N$ adopts a minimum. The corresponding dependence, $h^{eq}(p)$, is displayed in the inset. The solid line in the inset interpolates between the symbols, calculated at $p = 0$, 6, 12, and 18 Å. Note, our choice $\gamma = 0.08 k_B T/$Å^2 ensures the thickness of a bare, peptide-free membrane to be $h^{eq}(p = 0) = 26$ Å. The lipid/peptide ratio is $N = 80$.

$k_B T/$Å^2). With this value for γ, we show in Fig. 8 the free energy per lipid chain, $\triangle F/N$, as a function of h for a number of different peptide penetration depths, p. The optimal thickness shifts to smaller values for $p = 6$ Å (*curve* with *diamonds*), remains unaffected for $p = 12$ Å (*curve* with *arrowheads*), and becomes larger for $p = 18$ Å (*curve* with *stars*). The inset of Fig. 8 shows the equilibrium thickness, $h^{eq}(p)$, as a function of peptide penetration depth, p, emphasizing the nonmonotonic behavior of $h^{eq}(p)$. Note again that due to our choice of γ, it is $h^{eq}(p = 0) = h^* = 26$ Å.

The change in free energy upon membrane thinning is small if measured per lipid; for example, at $p = 6$ Å, we find $\triangle F(h = 26$ Å$) - \triangle F(h = 24$ Å$) = 0.063\, N k_B T$ (see Fig. 8). However, when measured per peptide (recall $N = 80$), we obtain $0.063\, k_B T \times 80 = 5\, k_B T$, which can be significant for the adsorption energetics of amphipathic peptides.

Binding energy of amphipathic peptides

Consider the transfer of a single amphipathic peptide from aqueous solution into a lipid membrane. The corresponding transfer free energy

$$\triangle F_{\rm tot} = \triangle F_{\rm sol} + \triangle F_{\rm lip} \tag{24}$$

can be written as a sum of two principal contributions (White and Wimley, 1998; Ben-Tal et al., 1996). One is the desolvation free energy, $\triangle F_{\rm sol}$, which results from changes in both electrostatic interactions and (nonelectrostatic) interfacial energies between the amino acid side chains of the peptide and the environment. A second contribution, $\triangle F_{\rm lip}$, expresses the peptide-induced perturbation of the lipid bilayer. Our approach in this study provides a molecular-level calculation of $\triangle F_{\rm lip}$.

Let us discuss how $\triangle F_{\rm lip}$ depends on the peptide penetration depth, p. Because the membrane can optimize its thickness $h = h^{\rm eq}$, we identify

$$\triangle F_{\rm lip} = \triangle F(p, h^{\rm eq}(p)) \tag{25}$$

measured per peptide (of length $D = 30$ Å). The curve with diamonds of Fig. 9 shows the peptide-induced perturbation of the lipid bilayer, $\triangle F_{\rm lip}$, measured per peptide, as a function of p, or, equivalently, as a function of the polar angle α (from the Theory section we recall the relation $p = r_{\rm P}[1 + \cos(\alpha/2)]$). For not too small p (Fig. 9 predicts $p > 1$ Å), we find the lipid membrane provides a contribution to the transfer free energy that increases with p (or, equivalently, decreases with α). That is, the perturbation induced by a peptide with polar angle $\alpha = 90°$ is larger than the perturbation induced by a peptide with polar angle $\alpha = 180°$.

A molecular-level calculation of the desolvation free energy, $\triangle F_{\rm sol}$, is outside the scope of this work. Still, we can very roughly estimate the p-dependence of $\triangle F_{\rm sol}$ that arises from varying the angular size, $2\pi - \alpha$, of the hydrophobic face. To this end, we assume that the peptide is positively charged, with all charged residues distributed over the polar helix face (which is of angular size α). Upon entry into the membrane, charged residues start penetrating into the hydrocarbon core for $p > r_{\rm P}[1 + \cos(\alpha/2)]$, and the electrostatic free energy becomes intolerably high. Let us—as

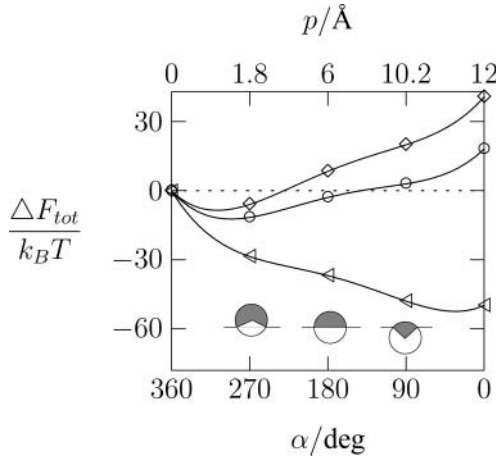

FIGURE 9 Transfer free energy, $\triangle F_{\rm tot}$, per peptide for $\gamma_{\rm P} = 0$ (◇), for $\gamma_{\rm P} = 0.02\, k_B T/$Å^2 (○), and for $\gamma_{\rm P} = 0.08\, k_B T/$Å^2 (◁), plotted as a function of the angular size, α, of the polar helix face (see Fig. 2). For $\alpha = 90°$, 180°, and 270°, we schematically picture the size of the polar face (*shaded regions*), indicating the corresponding peptide penetration into the membrane.

a crude approximation—neglect all other electrostatic contributions that arise from interactions of the lipid headgroups with the peptide and from solvation effects of the peptide's backbone dipoles (for detailed accounts of the solvation free energies, see, for example, Kessel and Ben-Tal, 2002). We thus assume that within the range $0 \leq p \leq r_P[1 + \cos(\alpha/2)]$, the electrostatic energy remains constant. The remaining (nonelectrostatic) interfacial energy between the peptide and the aqueous environment is proportional to the exposed contact area, $A_{exp} = (2\pi - \alpha)r_P D$, between the hydrophobic peptide face and the aqueous environment

$$\triangle F_{sol} \approx \gamma_P A_{exp} = \gamma_P(2\pi - \alpha)r_P D, \quad (26)$$

where γ_P is the corresponding surface tension. The magnitude of γ_P depends on the strength of the peptide's hydrophobicity. In Fig. 9, we plot $\triangle F_{tot}$ as a function of α for different values of γ_P (note that the curve with diamonds is derived for $\gamma_P = 0$ and thus corresponds to $\triangle F_{lip}$).

Fig. 9 suggests that for sufficiently small γ_P, namely, when the lipid perturbation dominates the interaction, the transfer free energy decreases with α (or increases with the penetration depth of the peptide, p). In fact, this finding is in line with the results of a recent experiment that was designed to investigate the influence of the polar angle on peptide adsorption (Wieprecht et al., 1997). The experimentally used model peptides all had similar structural properties (overall charge, hydrophobicity, and hydrophobic moment); they differed in the angle, α, subtended by the positively charged (and thus polar) helix face. It was found that peptide adsorption increases with α. Wieprecht et al. (1997) explained this result by the different interaction strengths between the hydrophobic faces of the different peptides and the aqueous environment. Indeed, different hydrophobicities of the involved amino acids are supposed to affect γ_P. Our complementary explanation derives from the lipid perturbation, induced by amphipathic peptides that penetrate into the hydrocarbon core of the lipid host. The corresponding free energy penalty, $\triangle F_{lip}$, increases with the penetration depth, p, of the peptide. Depending on the strength of the desolvation free energy, $\triangle F_{sol}$, even the total transfer free energy, $\triangle F_{tot}$, may increase with p and thus cause stronger membrane binding for peptides that penetrate less deeply into the membrane.

Hydrophobic peptides

For $\alpha = 0$, the peptide is completely hydrophobic, and the membrane penetration depth is $2r_P < p < h$. In this case, Fig. 8 predicts a thickening of the membrane rather than thinning (as for $P < 2r_p$). The increase in h is a direct consequence of the additional volume V_P occupied by the peptide within the membrane interior, without affecting the interfacial area $A = A_L$. The lipid perturbation free energy associated with fully inserting the hydrophobic peptide into the hydrocarbon core is shown by the curve with diamonds for $\alpha = 0$ in Fig. 9 (which is derived for $\gamma_P = 0$ and thus $\triangle F_{tot} = \triangle F$). Its amount $\triangle F(p = 2r_P) \approx 40 k_B T$ refers to the lipid's conformational free energy cost of inserting the peptide in horizontal orientation fully into the bilayer, measured relative to the unperturbed bilayer. Note, however, because the peptide is entirely hydrophobic, there is no longer a driving force to keep the peptide in horizontal orientation. Alternatively, it may adopt a vertical, transmembrane orientation to minimize the perturbation of the lipid bilayer. A transmembrane orientation may be particularly favorable if the length, D, of the peptide roughly matches the thickness, h, of the host membrane.

Let us estimate whether transmembrane orientation is more favorable than horizontal orientation. Assume that the condition $h \approx D$ applies. From previous calculations of the perturbation free energy of rigid (and sufficiently large) transmembrane inclusions (Fattal and Ben-Shaul, 1993; May and Ben-Shaul, 2000), we recall a value of $\approx 0.3 - 0.4\ k_B T$/1 Å length of the inclusion circumference. For a cylindrical rod of radius $r_P = 6$ Å in transmembrane orientation, this amounts to $\triangle F = 11 - 15\ k_B T$, which is much lower than the value for horizontal insertion. Even a certain amount of mismatch between D and h will easily be tolerated. Hence, our results suggest a strong preference of completely hydrophobic peptides for transmembrane orientation due to the generally large lipid perturbation free energy for horizontal insertion.

Recently, a completely hydrophobic ''inert'' model peptide, consisting of the helix-promoting leucine and alanine, was synthesized, and its interaction with lipid membranes was analyzed by Yano et al. (2002). Most remarkably, despite the lack of polar ''stabilizing'' residues at the ends, the peptide adopted a stable transmembrane orientation. Clearly, our calculations in this study suggest that the lipid bilayer provides a sufficiently large energetic incentive to stabilize the transmembrane orientation of hydrophobic α-helices.

Peptide concentration effects

So far, all results were derived for a fixed lipid/peptide ratio of $N = 80$. We now investigate the membrane properties as a function of N, which is an experimentally controllable parameter. To this end, we focus on peptides with angular size $\alpha = \pi$ of the polar part. This leads to a peptide penetration depth of $p = r_P = 6$ Å. We recall from Fig. 7 that this choice implies a particularly large conformational free energy $\triangle F_c$.

According to the numerical scheme described in the Theory section, we calculate the lipid perturbation free energy, F_c, for different peptide-peptide distances, L. For simplicity, we continue to assume the same geometry of the unit cell as introduced in the Theory section. That is, the

peptides form long, orientationally ordered arrays so that the membrane properties are invariant along the y direction (see Fig. 1), and the lipid/peptide ratio N relates to L through (see Eqs. 1 and 2)

$$N = (Lh - \frac{\pi}{2} r_P^2) \frac{D}{v}. \quad (27)$$

Note that Eq. 27 is not valid for $L \gg D$; we thus exclude the limit of small peptide concentrations from our discussion.

In Fig. 10 we show the excess free energy per peptide, $\triangle F$, as a function of $1/L$ for different membrane thicknesses, h. Note that Fig. 10 focuses on the range $20 < L/\text{Å} < 100$. For $L \lesssim 20$ Å (which corresponds roughly to $N = 20$), the peptide-peptide distance falls below the lateral extension of individual (double chained) lipids. Hence, at such small interpeptide separations, our continuum-like description of the lipids along the x axis must fail.

Because of the reference state, only the curve corresponding to $h = h^* = 26$ Å in Fig. 10 approaches a finite value in the low peptide concentration limit where $N \sim L \to \infty$. All other curves, derived for $h < h^*$, exhibit the limiting behavior $\triangle F(L \to \infty) = \infty$, which is a consequence of our assumption that the membrane thickness, h, is spatially constant everywhere. Yet, more interesting than the dilute limit is the intermediate region where L is on the order of D. Here, Fig. 10 clearly shows that membrane thinning lowers the peptide-induced free energy penalty of the membrane. The magnitude of the decrease in h depends on L. For each L there is a thickness $h^{eq}(L)$ that minimizes $\triangle F$. These values are displayed in Fig. 10 by the broken line. The broken line thus corresponds to the minimal excess free energy per peptide, $\triangle F$, with the optimization of the membrane thickness taken into account. The inset (*solid line*) shows the corresponding optimal thickness, h^{eq}, as a function of $1/N$, where the relation between L and N is calculated according to Eq. 27. The dependence $h^{eq}(1/N)$ shows a linear relation between membrane thickness and peptide/lipid ratio, $1/N$.

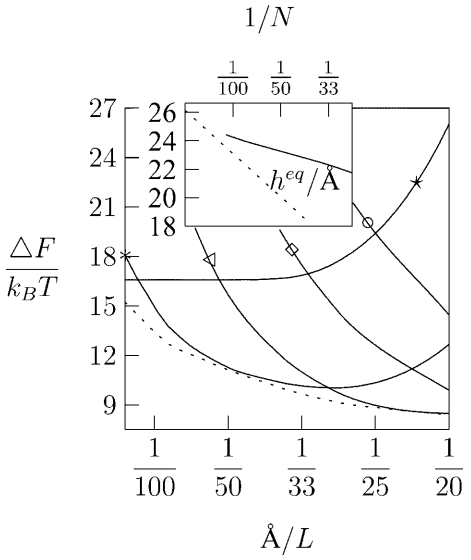

FIGURE 10 Excess free energy, $\triangle F$, per peptide rod, as a function of $1/L$ for $h = 18$ Å (○), $h = 20$ Å (◇), $h = 22$ Å (◁), $h = 24$ Å (*), and $h = 26$ Å (★). The broken line denotes the minimal value of $\triangle F$, calculated for optimal thickness, $h = h^{eq}(1/L)$. The corresponding values for the optimal thickness, h^{eq}, are shown in the inset as a function of peptide/lipid ratio, $1/N$ (*solid line*). The relation between N and L is given by Eq. 27. The broken line in the inset shows the prediction for $h = h^{eq}(1/N)$ according to Eq. 28 with $a_L = 31.2$ Å^2 and $a_P = 360$ Å^2. All results are derived for a peptide penetration depth of $p = r_P = 6$ Å.

Indeed, a linear decrease of membrane thickness with increasing peptide concentration has been measured experimentally (He et al., 1996; Ludtke et al., 1995). A simple rationale of this behavior was given as follows: assume that N_P membrane-associated peptides only increase the interfacial area, $2A = N_L a_L + N_P a_P$, of the bilayer (a_L and a_P are the fixed cross-sectional areas per lipid and peptide, respectively, measured at the membrane interface), whereas the entire hydrocarbon core (of volume $V = N_L v = Ah$) of the bilayer is filled with the tails of N_L lipids. In this case, the optimal membrane thickness

$$h = h^{eq} = \frac{2v}{a_L} \frac{1}{1 + a_P/(a_L N)} \approx \frac{2v}{a_L} \left(1 - \frac{1}{N} \frac{a_P}{a_L}\right) \quad (28)$$

decreases linearly with the peptide/lipid ratio $1/N = N_P/N_L$. Recall the numerical values $a_L = 2v/h^* = 31.2$ Å^2 and $a_P = 2r_P D = 360$ Å^2 (valid for $p = r_P = 6$ Å). The broken line in the inset of Fig. 10 shows $h^{eq}(1/N)$ according to Eq. 28. The difference in the two curves of the inset in Fig. 10 reflects the adjustment of the average cross-sectional area, a_L, per lipid chain upon association between membrane and peptide.

Fig. 10 reveals another notable result: The peptide-induced perturbation free energy, $\triangle F$, monotonically decreases with decreasing distance, L, between the peptides. Hence, two interfacially adsorbed peptides that are oriented in parallel experience an attractive, membrane mediated force. For a peptide length of $D = 30$ Å, the corresponding gain in free energy can be large compared to $k_B T$ (see Fig. 10). Hence, for a sufficiently large concentration of peptides in the membrane, we expect the separation into peptide-enriched and peptide-depleted phases. We do not attempt to calculate a phase diagram; instead we note that the phase boundaries will be modulated by additional forces that are not taken into account in the present approach; i.e., electrostatic repulsion between the (usually positively) charged residues of the peptides or the orientational entropy associated with the elongated (cylinder-like) shape of the peptides. We also note that the attraction between membrane-adsorbed peptides is expected to be less pronounced if local thickness modulations of the bilayer are taken into account (they are neglected in this work). Still, our results in

Fig. 10 clearly point at the active role that the membrane plays in the self-assembly of amphipathic peptides.

The reason for the membrane-mediated attraction of amphipathic peptides is somewhat similar than for transmembrane peptides or proteins. The latter are commonly discussed in terms of the hydrophobic mismatch between the thickness of the hydrophobic span of the peptide and that of the host bilayer (Gil et al., 1998; May, 2000). Here, membrane-spanning peptides impose a decrease (or, equivalently, increase) of the membrane thickness that decays with a typical length in the nanometer range. Upon decreasing the peptide-peptide distance, the perturbed lipid annuli of the peptides overlap. Typically then, the perturbation free energy per lipid increases, but the number of perturbed lipids decreases faster, implying attractive interactions between transmembrane peptides. Similarly, interfacially adsorbed peptides tend to decrease the membrane thickness, and—through this tendency—mediate attractive interactions to optimize the overall membrane perturbation.

CONCLUSIONS

Amphipathic peptides often occur as components of the defense system of animals and plants against microorganisms; they operate through an efficient membrane permeabilization that appears to involve cooperative peptide-peptide interactions. This work represents a molecular-level approach to calculate the perturbation free energy induced by partially membrane-inserted amphipathic peptides. In agreement with experimental results, we predict a characteristic decrease in the molecular order of the lipid chains, peptide-induced membrane thinning, and a membrane binding energy of amphipathic peptides that decreases with the angular size of the peptide's polar face. In addition to that, we predict membrane-mediated attractive interactions between partially membrane-inserted amphipathic peptides. And finally, for completely hydrophobic peptides, our results point at a strong preference of a transmembrane orientation rather than a horizontal insertion into the apolar membrane core.

Our results are based on a number of approximations, such as the mean-field nature of the underlying chain-packing theory and, particularly, the assumption of membrane flatness and uniform bilayer thickness everywhere. For this investigation, these assumptions are not expected to alter our (qualitative) conclusions. Yet, to study the activity of amphipathic peptides regarding membrane destabilization, local curvature and thickness modulations should be accounted for.

This study is mainly concerned with horizontally adsorbing peptides in the membrane interface. It is natural to extend this study and to focus on the transition from the adsorbed to the inserted state, where the peptides constitute the walls of water-filled pores. This will be done in a forthcoming report where we will also account for local curvature modulations.

We thank Dr. Klaus Gawrisch for fruitful discussions. S.M. thanks the Thüringer Ministerium für Wissenschaft, Forschung und Kunst. A. Z. thanks the Yeshaya Horowitz Foundation for a doctoral fellowship.

The financial support of the Israel Science Foundation and the United States-Israel Binational Science Foundation is gratefully acknowledged. The Fritz Haber Center is supported by the Minerva Foundation, Munich, Germany.

REFERENCES

Aranda-Espinoza, H., A. Berman, N. Dan, P. Pincus, and S. A. Safran. 1996. Interaction between inclusions embedded in membranes. *Biophys. J.* 71:648–656.

Bechinger, B. 1997. Structure and functions of channel-forming peptides: magainins, cecropins, melittin and alamethicin. *J. Membr. Biol.* 156: 197–211.

Bechinger, B. 1999. The structure, dynamics and orientation of antimicrobial peptides in membranes by multidimensional solid-state NMR spectroscopy. *Biochim. Biophys. Acta.* 1462:157–183.

Bechinger, B. 2001. Solid-state NMR investigations of interaction contributions that determine the alignment of helical polypeptides in biological membranes. *FEBS Lett.* 504:161–165.

Ben-Shaul, A. 1995. Molecular theory of chain packing, elasticity and lipid protein interaction in lipid bilayers. *In* Structure and Dynamics of Membranes, Vol. 1A. R. Lipowsky and E. Sackmann, editors. Elsevier, Amsterdam. 359–402.

Ben-Tal, N., B. Honig, R. M. Peitzsch, G. Denisov, and S. McLaughlin. 1996. Binding of small basic peptides to membranes containing acidic lipids: theoretical models and experimental results. *Biophys. J.* 71: 561–575.

Chen, F. Y., M. T. Lee, and H. W. Huang. 2003. Evidence for membrane thinning effect as the mechanism for peptide-induced pore formation. *Biophys. J.* 84:3751–3758.

Dathe, M., and T. Wieprecht. 1999. Structural features of helical antimicrobial peptides: their potential to modulate activity on model membranes and biological cells. *Biochim. Biophys. Acta.* 1462:71–87.

Epand, R. M. 1997. Modulation of lipid polymorphism by peptides. *Curr. Top. Membr.* 44:237–252.

Epand, R. M., and H. J. Vogel. 1999. Diversity of antimicrobial peptides and their mechanisms of action. *Biochim. Biophys. Acta.* 1462:11–28.

Fattal, D. R., and A. Ben-Shaul. 1993. A molecular model for lipid protein interaction in membranes: The role of hydrophobic mismatch. *Biophys. J.* 65:1795–1809.

Gil, T., J. H. Ipsen, O. G. Mouritsen, M. C. Sabra, M. M. Sperotto, and M. J. Zuckermann. 1998. Theoretical analysis of protein organization in lipid membranes. *Biochim. Biophys. Acta.* 1376:245–266.

Hancock, R. E. W., T. Fella, and M. Brown. 1995. Cationic bactericidal peptides. *Adv. Microb. Physiol.* 37:135–175.

Harroun, T. A., W. T. Heller, T. M. Weiss, L. Yang, and H. W. Huang. 1999. Theoretical analysis of hydrophobic matching and membrane-mediated interactions in lipid bilayers containing gramicidin. *Biophys. J.* 76:3176–3185.

He, K., S. J. Ludtke, W. T. Heller, and H. W. Huang. 1996. Mechanism of alamethicin insertion into lipid bilayers. *Biophys. J.* 71:2669–2679.

Hristova, K., C. E. Dempsey, and S. H. White. 2001. Structure, location, and lipid perturbations of melittin at the membrane interface. *Biophys. J.* 80:801–811.

Huang, H. W. 1986. Deformation free energy of bilayer membrane and its effect on gramicidin channel lifetime. *Biophys. J.* 50:1061–1070.

Huang, H. W. 1995. Elasticity of lipid bilayer interacting with amphiphilic helical peptides. *J. Phys. II France.* 5:1427–1431.

Jing, W., H. N. Hunter, J. Hagel, and H. J. Vogel. 2003. The structure of the antimicrobial peptide Ac-RRWWRF-NH2 bound to micelles and its interactions with phospholipid bilayers. *J. Pept. Res.* 61:219–229.

Kessel, A., and N. Ben-Tal. 2002. Free energy determinants of peptide association with lipid bilayers. *In* Current Topics in Membranes: Peptide-Lipid Interactions, Vol. 52. S. Simon and T. McIntosh, editors. Academic Press, San Diego. 205–253.

Koenig, B. W., J. A. Ferretti, and K. Gawrisch. 1999. Site-specific deuterium order parameters and membrane-bound behavior of a peptide fragment from the intracellular domain of HIV-1 gp41. *Biochemistry.* 38:6327–6334.

Lin, J.-H., and A. Baumgärtner. 2000. Stability of a melittin pore in a lipid bilayer: a molecular dynamics study. *Biophys. J.* 78:1714–1724.

Ludtke, S. J., K. He, and H. W. Huang. 1995. Membrane thinning caused by magainin 2. *Biochemistry.* 34:16764–16769.

Matsuzaki, K. 1999. Why and how are peptide-lipid interactions utilized for self-defense? Magainins and tachyplesins as archetypes. *Biochim. Biophys. Acta.* 1462:1–10.

May, S. 2000. Theories on structural perturbations of lipid bilayers. *Curr. Op. Coll. Int. Sci.* 5:244–249.

May, S., and A. Ben-Shaul. 1999. Molecular theory of lipid-protein interaction and the L_α-H_{II} transition. *Biophys. J.* 76:751–767.

May, S., and A. Ben-Shaul. 2000. A molecular model for lipid-mediated interaction between proteins in membranes. *Phys. Chem. Chem. Phys.* 2:4494–4502.

Münster, C., A. Spaar, B. Bechinger, and T. Salditt. 2002. Magainin 2 in phospholipid bilayers: peptide orientation and lipid chain ordering studied by x-ray diffraction. *Biochim. Biophys. Acta.* 1562:37–44.

Nicolas, P., and A. Mor. 1995. Peptides as weapons against microorganisms in the chemical defense system of vertebrates. *Annu. Rev. Microbiol.* 49:277–304.

Nielsen, C., M. Goulian, and O. S. Andersen. 1998. Energetics of inclusion-induced bilayer deformations. *Biophys. J.* 74:1966–1983.

Oren, Z., and Y. Shai. 1998. Mode of action of linear amphipathic alpha-helical antimicrobial peptides. *Biopolymers.* 47:451–463.

La Rocca, P., P. C. Biggin, D. P. Tieleman, and M. S. P. Sansom. 1999. Simulation studies of the interaction of antimicrobial peptides and lipid bilayers. *Biochim. Biophys. Acta.* 1462:31–40.

Saiz, L., S. Bandyopadhyay, and M. L. Klein. 2002. Towards an understanding of complex biological membranes from atomistic molecular dynamics simulations. *Biosci. Rep.* 22:151–173.

Shepherd, C. M., H. J. Vogel, and D. P. Tieleman. 2003. Interactions of the designed antimicrobial peptide MB21 and truncated dermaseptin S3 with lipid bilayers: molecular-dynamics simulations. *Biochem. J.* 370: 233–243.

White, S. H., and W. C. Wimley. 1998. Hydrophobic interactions of peptides with membrane surfaces. *Biochim. Biophys. Acta.* 1376: 339–352.

Wieprecht, T., M. Dathe, R. M. Epand, M. Beyermann, E. Krause, W. L. Maloy, D. L. MacDonald, and M. Bienert. 1997. Influence of the angle subtended by the positively charged helix face on the membrane activity of amphipathic, antibacterial peptides. *Biochemistry.* 36:12869–12880.

Yamaguchi, S., D. Huster, A. Waring, R. I. Lehrer, W. Kearney, B. F. Tack, and M. Hong. 2001. Orientation and dynamics of an antimicrobial peptide in the lipid bilayer by solid-state NMR spectroscopy. *Biophys. J.* 81:2203–2214.

Yano, Y., T. Takemoto, S. Kobayashi, H. Yasui, H. Sakurai, W. Ohashi, M. Niwa, S. Futaki, Y. Sugiura, and K. Matsuzaki. 2002. Topological stability and self-association of a completely hydrophobic model transmembrane helix in lipid bilayers. *Biochemistry.* 41:3073–3080.

Zemel, A., D. R. Fattal, and A. Ben-Shaul. 2003. Energetics and self-assembly of amphipathic peptide pores in lipid membranes. *Biophys. J.* 84:2242–2255.

Zuckermann, M. J., and T. Heimburg. 2001. Insertion and pore formation driven by adsorption of proteins onto lipid bilayer membrane-water interfaces. *Biophys. J.* 81:2458–2472.